sustainability

MDPI

Article

Determination of the Small-Scale Physical Model Parameters of Pavement Structure

Veronika Valašková [1,*], Jozef Vlček [2] and Daniel Papán [1]

[1] Department of Structural Mechanics and Applied Mathematics, Faculty of Civil Engineering, University of Zilina, Univerzitna 8215/1, 010 26 Zilina, Slovakia; daniel.papan@uniza.sk
[2] Department of Geotechnics, Faculty of Civil Engineering, University of Zilina, Univerzitna 8215/1, 010 26 Zilina, Slovakia; jozef.vlcek@uniza.sk
* Correspondence: veronika.valaskova@uniza.sk; Tel.: +421-41-513-5606

Received: 27 October 2020; Accepted: 14 November 2020; Published: 18 November 2020

Abstract: A large amount of the local and first-class road infrastructures in Central Europe lead through settled areas, such as villages or even historical cities and town centers. The vibrations generated by passing vehicles around the pavement spread to the subgrade to the environment and also affect civil engineering structures and buildings. We have decided to adopt the approach of small-scale modeling of the pavement with the subgrade. Small-scale physical modeling brings benefits, such as size reduction, simplification, or controlled conditions during the test. To study the effect of static and dynamic behavior during the occurrence, a simulation mass physical model is used for testing. A static plate load test is used to determine the bearing capacity and settlement and consistency of measurement of the plate's vertical movement at a given load acting on the plate. The aim of the mass surface simulation's dynamic testing was to measure the response in time acceleration forms. Based on the performed experimental measurements undertaken on the physical model as well as the numerical simulation performed in FEM, we can state that the gelatin-based simulation mass is usable for the simulation of the earth environment in contact with building structures.

Keywords: small-scale physical model; static plate load test; dynamic testing of simulation mass

1. Introduction

The interaction between the vehicle and pavement makes up the main part of the research, and its consequences are being addressed by engineers around the world [1]. In general, the vehicle–pavement interaction system consists of two individual systems. Even though this phenomenon's solution may seem simple, the final solution is actually complex when a wider range of factors are involved. The vehicle, as a separate part of the interaction system, can be characterized as a very complicated dynamic system. Therefore, the combination of a vehicle–pavement system is difficult to describe exactly by the mathematical method.

A large amount of local and first-class road infrastructures in Central Europe lead through settled areas, such as villages or even historical city and town centers, as a remnant of the historical roads in past times. However, a large part of the traffic stays in settled areas because new road infrastructure is still absent in some localities. Local communications cannot keep up with the increasing traffic load, which leads to the degradation of the pavement parameters and the deterioration of the environment. In many cases, the service life of the pavements is exceeded, then defects and failures occur, which ultimately leads to the occurrence of stochastic sources of excitation for the dynamic vehicle–pavement system.

In an ideal load condition, when the vehicle is moving on a smooth surface, the dynamic behavior of the system can be described trivially by the mathematical expression of the problem [2,3].

One of the important parts of the vehicle–pavement interaction system is the pavement. In dynamic analyses, the pavement is often idealized or replaced by simpler variants, such as an elastic half space with general parameters. The task of solving the problem of the pavement can also be extended by the subsoil, which represents an important role in this interactive task.

The vibrations generated by a passing vehicle around the pavement spread to the subgrade environment and also affect the civil engineering structures and buildings. Limiting the spread of vibrations to the pavement and subsoil is very complicated due to the necessary heavy tracks and traffic in our infrastructure and diversity. Rehabilitation of the pavement stressed by dynamic phenomena focuses on eliminating the source of dynamic excitation and reducing its impact [4–6].

Therefore, this phenomenon needs to be solved, and a detailed investigation into the pavement is necessary. Observing the behavior of the pavement and subsoil on real structures is possible but very complicated due to the permanent involvement of measurement instrumentation in the construction phase and observation equipment thereafter. Considering the above-mentioned statements, the complexity of the phenomenon requires some generalization level without affecting the reliability of outputs [7,8]. For this reason, we have decided to adopt the approach of small-scale modeling of the pavement with the subgrade.

2. Road Infrastructure–Environment Interaction Analysis

2.1. Road Infrastructure Effect

Undoubtedly, the negative effect of the traffic on the surrounding environment is one of the most important tasks to solve. The negative effects involve various factors, such as vibrations, noise and air pollution, the risk of health injures, loss of life, or property damage [9–12]. The aim is to analyze the vibrating effect of traffic on buildings. Vibrations have a negative influence on the condition of buildings [13–15]. The change in stress peaks leads to fatigue of structural elements. Masonry or concrete members are especially predisposed to failure occurrences. Cracks or discontinuities in non-bearing elements are typical for excessive loads from traffic. Additionally, long-term effects of vibration have negative impacts on the health of inhabitants.

Besides the published works, the study is based on the in-situ observations of the authors. The locality is affected by heavy traffic, which inflicts failures in the non-bearing members of nearby buildings. The level of the road is higher than the entrances to the houses. This difference is secured by the concrete retaining wall along the communication supported by the concrete ribs connected with the buildings' foundation (Figure 1a).

(a) **(b)**

Figure 1. Supporting rib of the retaining wall along the communication: (**a**) The rib without interruption; (**b**) Interrupted rib at the house foundation.

The influence of traffic is intensified by the increasing extensiveness of pavement unevenness and irregularities. In this case, the settlement of sewer inlets created an obstacle in the track of the wheels. The impact of the tire on the inlet induces an increase in the loading amplitude. Insufficient technical conditions of the vehicles bring another deterioration of the state. An assumed major contribution of the rigid concrete rib led to a proposal to disconnect the rib and the foundation. Some of the ribs were modified in this way (Figure 1b).

Velocities in all three directions were measured at selected sites near the road: on the top of the retaining wall, on the rib, and in a pit below the rib. The values of the effective velocity in a particular direction lay in the interval from 0.01 to 0.24 mm·s^{-1}. The typical propagation of the velocity during the measurement is plotted in Figure 2. The energy of vibrations was evaluated through effective values of velocity instead of peak values, which only occur occasionally. The effective values better describe the overall energy potential of the wave and its influence.

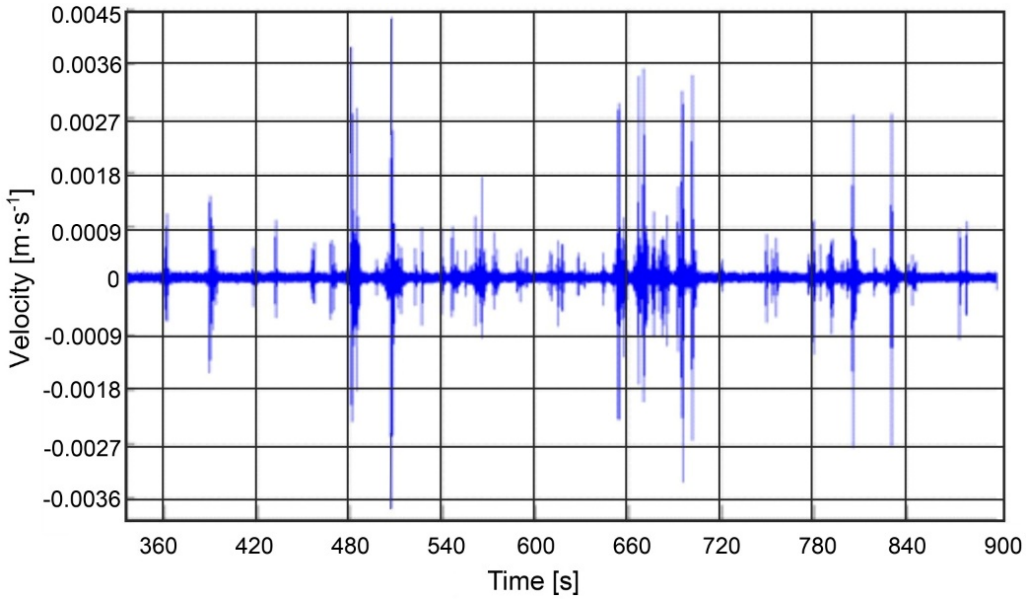

Figure 2. Time propagation of velocity of vibration at the top of the retaining wall in the vertical direction. Effective velocity $v_{(RMS)}$ = 0.154 mm·s^{-1}.

According to Eurocode 8, the structures subjected to seismic effects are evaluated by the maximum effective velocity at the foundation. For these types of buildings, the limit value is $v_{(RMS)}$ = 1.0 mm·s^{-1} [16]. While the overall stability is not threatened by the technical seismicity, some failures, such as cracks, may occur in non-bearing elements.

The ground and the building's frequency response sometimes leads to the strongest perception of the dynamic events. Thus, dominant frequencies were investigated. The typical propagation of the dominant frequencies is plotted in Figure 3.

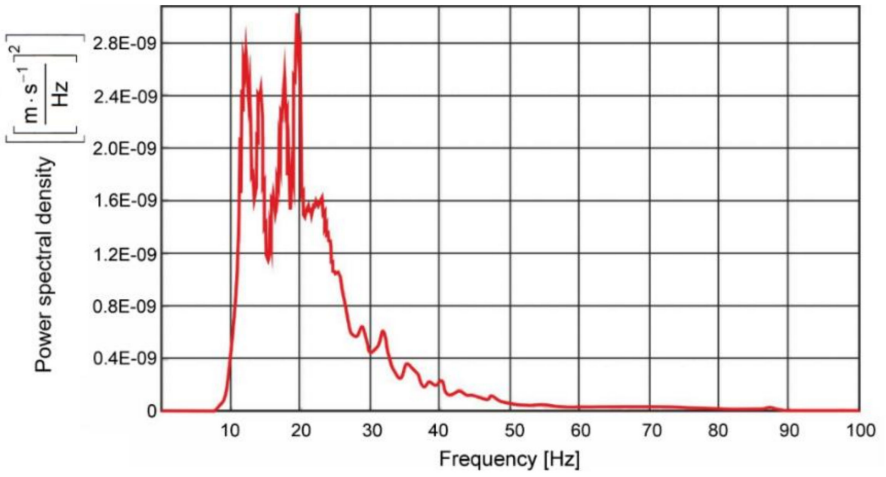

Figure 3. Power spectral density at the top of the retaining wall in the vertical direction; $f_{(max)}$ = 19.46 Hz.

The dominant frequencies varied from 8.9 to 22.5 Hz. This is a typical interval for a road traffic load. Typical dominant frequencies of masonry family houses are 2 to 6 Hz, so the resonant state of the buildings is not reached [17].

Measurements on the disconnected ribs showed some increase in the velocity. We assumed that the rigidity of the rib helps to reduce the energy of the wave. Disconnections of the rib did not influence the remediation of the state; even the polystyrene inlay did not work. A huge part of the vibration energy advanced through the ground and further below the building foundation. Accordingly, the ground represents an important part of the vibration transfer mechanism, and its investigation was the main goal in this study during the physical modeling.

2.2. Small-Scale Physical Modeling

Small-scale physical modeling brings benefits, such as size reduction, simplification, or controlled conditions during the test [18–24]. Partial problems can be investigated to verify the proposed hypothesis. On the other hand, some limitations should be taken into account: It is difficult to adopt the full behavior of the structure; more elements or partial mechanism aimed modeling is applicable; preparation of the test stand should be implemented at all know inputs.

The scaling has different influences on the parameters of the test. Some of them had a length of *1/n*, which was smaller on the scale than in reality. The area was $1/n^2$ smaller. The stress observed during the test was the same as in real structure. Table 1 contains the scaling factors for the usual quantities.

Table 1. Scaling effect.

Parameter		Dimension	Scale 1:n
length	L	m	1:n
area	A	m^2	$1:n^2$
force	F	N	$1:n^2$
stress	$\sigma = F/A$	N/m^2	1:n
one dimensional stiffness	F/L	N/m	1:n
settlement/distance		m/m	1:1

The scaling also depends on the test approach. Table 2 shows a comparison of scale factors for 1-g and centrifuge environments. Small-scale physical models have limitations in inducing sufficient stress levels, so constitutive behavior of the soil can be affected. Centrifuge apparatus creates an enhanced gravity field to compensate for the low stresses.

Table 2. Scaling factors for 1-g and centrifuge physical modeling [24].

Parameter	Scale Factor	
length	n	
area	n^2	
force	n^2	in centrifuge
	$N \cdot n^2$	in other cases
stress	1	in centrifuge
	N	in other cases
displacement	n	
strain	1	

Where N is the stress scale factor, and x is the geometric scale ratio.

These measures solve the task from a static point of view, but the dynamic behavior of the structure makes the task more complex. Besides the scale transformation, the test materials' properties have a significant influence on the model output. A simple conversion of quantities using the implemented scale mentioned above leads to unreliable results [22]. The behavior of the materials at such a small scale is not linearly dependent on the scale factor. Some corrections are then required to obtain usable results. Additionally, the "dynamic" behavior of the test material itself should be taken into account. The properties are often stress-, frequency-, or time-dependent. The application of proper material depends on the purpose of the physical modeling and desired scale factor.

Considering the effect of the traffic load on the pavement subgrade, the effect of a vehicle passing has a short duration, and the subgrade and also layers of the pavement should be described by the dynamic parameters. In terms of overall test conditions, the "apparent" behavior of the test material becomes important at any given load, time, and frequency interval. The overall response of the subgrade should match the prerequisites taken from the in-situ measurements. Partial parameters of the test material do not have to fit the scaling rule if the above-mentioned condition is fulfilled.

Besides the investigation of specific parameters of the selected simulation mass for the subgrade, we kept in mind the overall response of the mass to the traffic load and its potential utilization for various test conditions, such as scale factor, load level, or frequency spectrum.

3. Simulation Mass Material Properties

A physical model of simulation mass was used for testing to study the effect of static and dynamic behavior during the occurrence. A gelatin-based material was chosen for the needs of physical modeling, whereas the material parameters of this material were very suitable for the approximation of the dynamic behavior of soil materials [25]. Physical models that use the viscoelastic properties of modeling materials are suitable for modeling dynamic phenomena in rock environments, such as pavement subgrades. This realistic prototype scale model was simplified to define the small-scale model.

3.1. Material Properties

The bulk density determined on the test material sample was 1200 kg/m^3 at a standard ambient temperature of 20 °C. Poisson's ratio was 0.5 for the given material.

3.1.1. Infrared Spectroscopy

Infrared spectroscopy belongs to the group of non-destructive analytical methods, where the examined sample is not damaged in any way by the analysis while providing information about its composition. The obtained values of vibrational energies were related to the strength of chemical bonds and also to the molecular geometry with molecular structure. Although infrared spectroscopy is used in the analysis of macroscopic samples, its essence is the interaction of microparticles (molecules) forming this macroscopic sample with infrared radiation. The main focus of infrared spectroscopy is the interaction of infrared radiation with the studied sample. By infrared radiation, we mean

electromagnetic radiation in the wavelength range 20 to 12,500 cm^{-1} and wavelengths of 0.5 nm to 800 mm.

When infrared radiation interacts with a molecule, only the radiation whose energy corresponds to the difference between the individual vibrational levels of the respective oscillator is absorbed or emitted. If the current source frequency corresponds to a certain energy level difference, absorption occurs, and an absorption band appears in the infrared spectrum. The infrared spectrum of a substance represents the dependence of permeability T, absorbance A, reflectance on the wavenumber R, and wavelength λ,

$$T = \frac{\Phi}{\Phi_0}; \quad A = log\,\frac{\Phi_0}{\Phi}; \qquad R = \frac{\Phi_{reflected}}{\Phi_0} \tag{1}$$

where Φ_0, Φ reflections represent the flux of radiation in front of and behind the cuvette and the flux of radiation reflected by the sample [26,27].

3.1.2. Material Sample Tested with Infrared Spectroscopy

Infrared absorption measurements were carried out with an FTIR Spectrometer Nicolet 5700 suitable for the widest range of analytical applications. For diagnostic purposes, a portion of the sample was taken and tested using this technology. Infrared spectrum of the tested sample is shown in Figure 4.

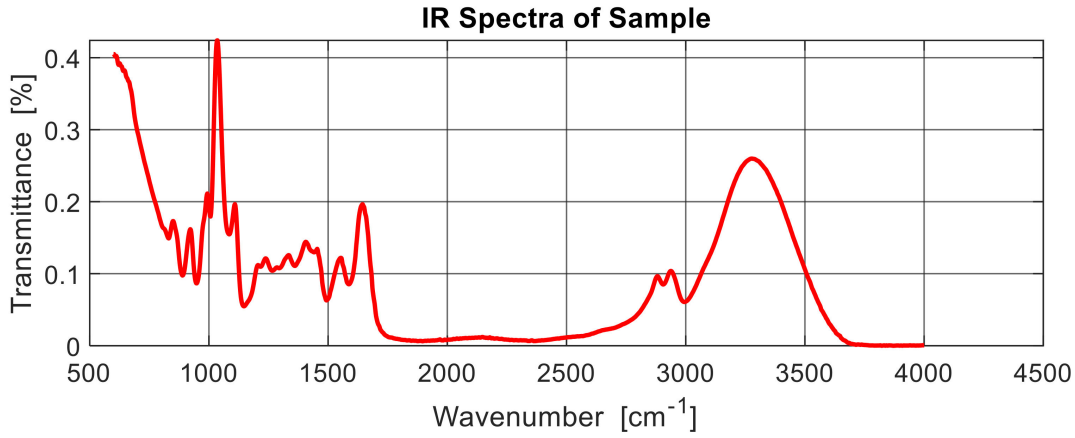

Figure 4. Infrared (IR) spectrum of the tested sample.

Relatively sharp absorption bands throughout the mid-infrared (IR) region from 4000 to 550 cm^{-1} characterize the IR spectrum of the sample. Much wider absorption bands were visible in amorphous trehalose. The sample showed the presence of one sharp band around 3350 cm^{-1} and a few shoulder peaks in the OH stretching region between 3100 and 2600 cm^{-1} that are indicative of hydrogen bonds of defined geometric positions, see Figure 4. The broad features of the OH band of the amorphous trehalose indicated a wide range of hydrogen-bond lengths and orientations. In the area of stretching C-H of the range 3000 and 2600 cm^{-1}, it was possible to identify bands. These FIR results are characteristic for glycerol - 98% - nonaromatic alcohol [28,29]. The shape of the region between 1700 and 1100 cm^{-1} describes peaks consisted of six local peaks. The increase in absorbance at 1630 cm^{-1} may also be associated with the formation of deformation bands of adsorbed water molecules. The amide II region (deformation vibrations -CN and -CNH) was less sensitive to changes in the secondary structure than amide I but was strongly affected by hydration. A comparison of the IR spectra of the tested sample and dedicated chemical element can be seen in the Figure 5. This course and scattering are characteristic of the material composition of gelatin mixture on a natural basis [30,31].

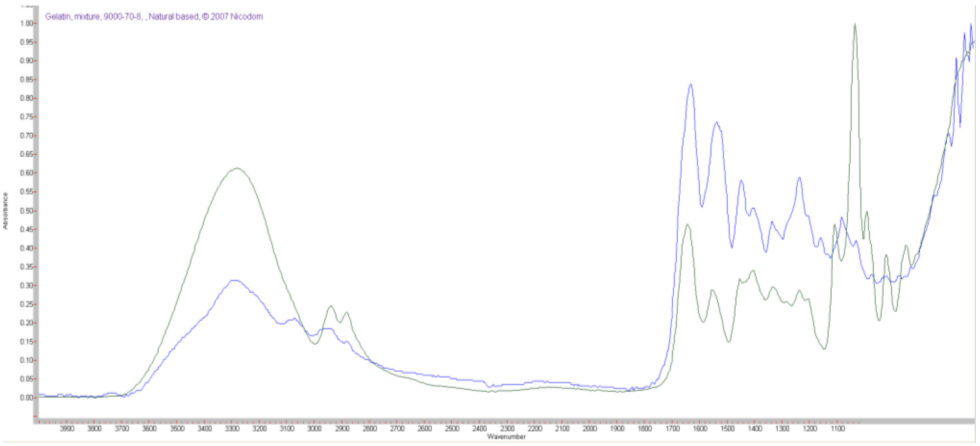

(a)

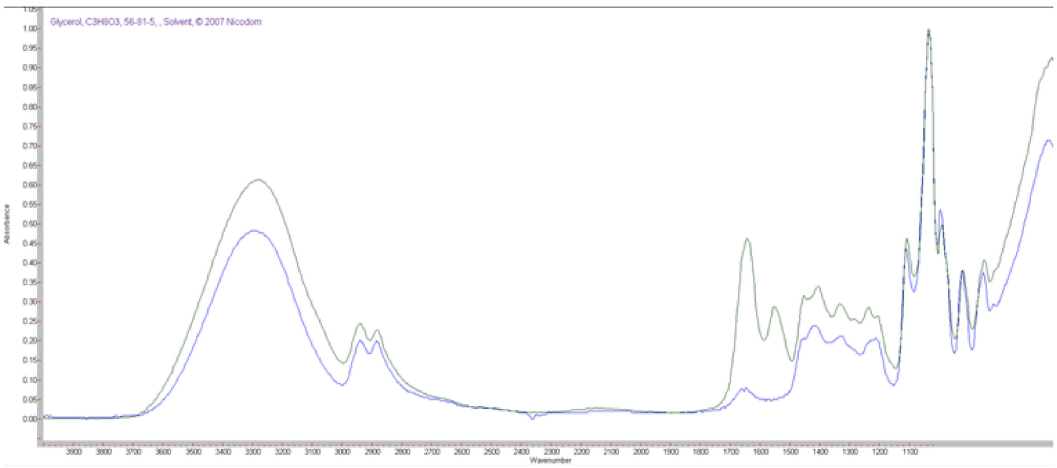

(**b**)

Figure 5. IR spectrum of the tested sample compared with (**a**) Gelatin; (**b**) Glycerol.

3.2. Methodology

However, the real behavior of the vehicle–pavement interaction system is more complicated as it is influenced by factors, such as

- The degree of generalization of the real vehicle to the model;
- The non-homogeneity of the masses and their distribution in the vehicle;
- The difficult estimation of the dynamic parameters of the vehicle subsystems, such as stiffness, damping, etc.;
- Additional excitation sources from the moving vehicle part, such as clutch, gearbox, other engine parts, or suspension;
- The change in the dynamic parameters due to the change in temperature, humidity, or aging processes;
- The material parameters of the pavement layers and the subgrade and their inhomogeneity and imperfections;

- The change in parameters in time due to the temperature, humidity, or other phenomena, such as groundwater flow or flooding;
- The harmonic and stochastic unevenness of the pavement surface;
- Defects and failures in the pavement, such as potholes, cracks, or sinkholes;
- Other factors, including retarders or joints.

3.3. Numerical and Theoretical Approach

For the best evaluation of experimental measurements, it is a very suitable step to create a numerical model. In the Adina computational system based on the finite element method, a pre-primary computational model was created, which served as the first approximation to the real physical model. This model was created under the assumption of a linearly elastic homogenous material for small deformations. Hence, the relative deformations in the initial stages of the experimental determination of experimental characteristics can be deduced. The model was composed of a solid type of 3D finite element, and a static analysis was performed. The numerical model's boundary conditions were chosen to accurately reflect the real state of the physical model. The degrees of freedom taken from the undersides and bounders ides of the model should reflect the metal container's behavior. In Figure 6, the 3D finite element numerical model is shown. The model will still be calibrated and will be used for future research in static and dynamic analyses.

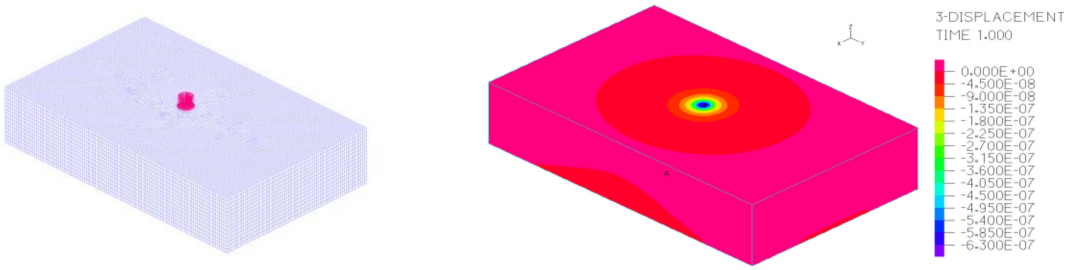

(a) **(b)**

Figure 6. (**a**) 3D mesh model with load; (**b**) Course of deformation static analysis of the model.

To describe the behavior of viscoelastic materials, differential equations of the simplest rheological models are most often used in static or dynamic loads. The simplest model of viscoelastic material consists of a linear spring representing elasticity and a linear (Newtonian) damper representing viscosity. These basic elements can be combined either serially (Maxwell model) or in parallel (Voigt model). The static tests presented in this paper show that the material used as the simulation mass can be represented by the Maxwell material model.

4. Real Testing Stand

4.1. Test Stand Parameters

To test the simulation mass, a steel tank was assembled. The mass was poured into the tank after warming. The mass was then leveled to create a flat surface. The stand was stored in a room with a stable ambient temperature of 20 °C. Gelatin-like materials are sensitive to temperature changes when their viscosity varies. Because of the dynamic nature of testing, the steel tank was placed on rubber damping pads to reduce the influence of the vibrations traveling from the actuator, which served as a testing apparatus along the steel frame to the floor.

The steel frame was mounted above the tank without any direct contact with it. The testing apparatus was attached to the steel frame, and its height above the mass surface was adjusted in terms of test conditions. The scheme and geometric parameters are displayed in Figure 7.

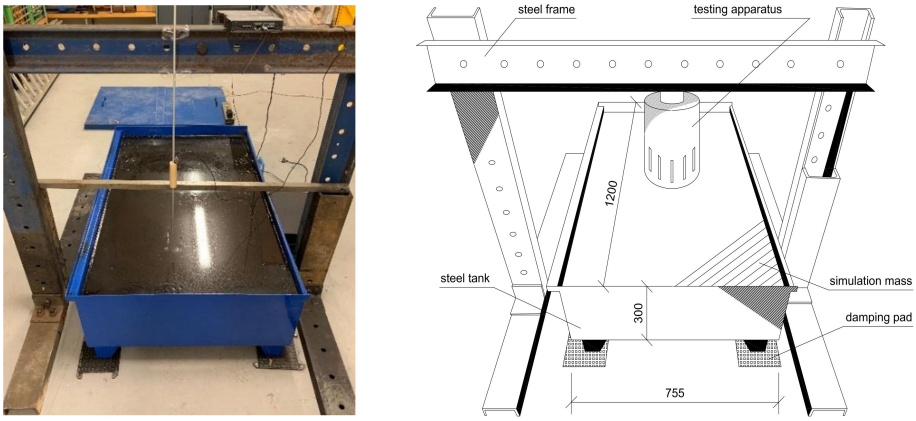

(**a**) (**b**)

Figure 7. Test stand: (**a**) Basic arrangement for measurements; (**b**) Scheme with the testing apparatus. Dimensions in millimeters.

The test apparatus and the whole steel frame could be positioned so that static and dynamic testing could be carried out at any point on the simulation mass. The steel frame was constructed using heavy steel U profiles to provide sufficient rigidity of the structure and to avoid the excessive vibration effects from the actuator.

4.2. Quasistatic Tests

For the purpose of material identification in terms of static parameters, static tests were performed on a small-scale physical model. Numerous variations of static testing can be applied to real structures. A standard static plate load test was performed due to the physical model's geometry and material parameters. It is a non-destructive method for determining the static strength of a material. The static plate load test with a diameter of 60 mm was completed in 5 measurement cycles.

The static plate load test is used to determine the bearing capacity and settlement, which consists of measuring the plate settlement at a given load acting on the plate. If we know the boundary conditions as the diameter of the circular plate r and the absolute value of the proportion of relative deformations μ, we are able to calculate the modulus of elasticity E for the given pressure interval under the plate Δp and the corresponding elastic plate settlement y_e [32].

$$E_{inf} = \left[0.5 \cdot \pi \cdot \left(1 - \mu^2\right) \cdot \Delta p \cdot r\right] / y_e \quad (2)$$

The circular load plate with a diameter of 60 mm was made of wood, had a thickness of 15 mm, and a weight of 156 g. The circular plate was characterized by its rigidity and lightness as well. Hardened plexiglass with a diameter of 120 mm was placed on this circular plate. This plexiglass was used as a rigid body, from which the measured values could be subtracted from digital indicators. Both plates were placed on the test apparatus, which made it possible to load and lighten the test material. The measuring device used for static testing was a strain gauge used as a sensor to indirectly measure the mechanical stress on the surface of a part by measuring and its deformation. Digital indicators were used to subtract the deformation values. The equipment consisted of one whole facility and was installed on a rigid steel frame. Moreover, the vehicle wheel's dynamic load acts only for a short period, and a longer loading stage gives underestimated values of the modulus of elasticity.

For this reason, the static test was performed for a period of 30 s. The scheme of the static load test is displayed in Figure 8.

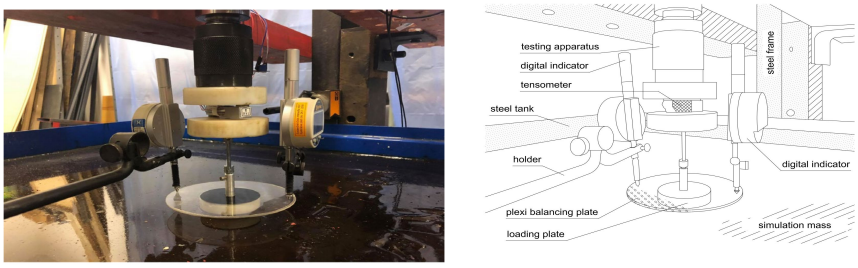

(a) **(b)**

Figure 8. Arrangement for quasistatic load test: (**a**) Measurement unit with digital indicators; (**b**) Scheme of the equipment.

4.3. Dynamic Tests

The simulation mass surface's dynamic testing aimed to measure the response in time acceleration forms. The analysis of the recorded data was focused on the frequency sensitivity of the investigated area and the damping. For this purpose, including surface wave propagation characteristics, the polar system of the sensor positions was created. The dimensions and the positions of the sensors in the polar net can be seen in Figure 9. Because the experiment holds the assumption of homogeneity, geometrical symmetry, and border conditions, the circular quadrant of the investigated area was selected. In this figure, the real experimental setup photo with accelerometers connections and measuring central can also be seen. Brüel and Kjær in-labo measuring equipment for the dynamic testing was used. The system BK Pulse with all modules is a powerful tool for measurements of all vibration types [33,34]. The specific members of the measuring line were

- 18 pcs—Accelerometers BK 4508B–002, CCLD variants are equipped with TEDS (transducer electronic data sheet) with original mounting Clip UA-1407 fixed to special light, stiff plastic foil;
- 18 pcs—AO-0038 Super low-noise, single-screened cable with 10–32 UNF connectors;
- 3 pcs—6-channel Input Module Type 3050, 51.2 kHz, in a BK original power frame Type 3660-C-100,
- A Laptop HP EliteBook with full BK Pulse system installed, connected to power frame with LAN cable.

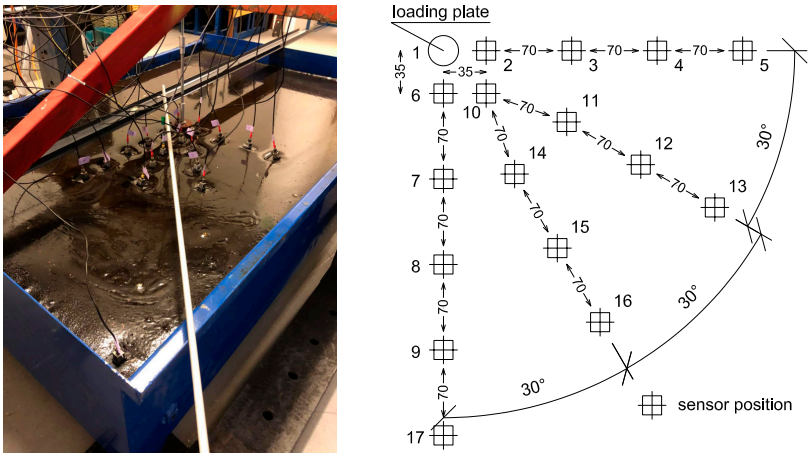

(a) **(b)**

Figure 9. Arrangement for dynamic testing: (**a**) Test equipment layout; (**b**) Scheme of the sensors' position; Distance of sensors in mm.

The vibration excitation was applied to the surface in the middle of the rectangle area through the rigid thick disc with a diameter of 40 mm (plastic plate). The reference accelerometer was situated near the center of this part of the excitation line. Additionally, this part was connected to an exciter with a rectification steel rod to ensure the ideal forced excitation. The excitation line consisted of the following parts:

- A TIRA Vibration exciter S 51110 fixed to the massive steel frame over the simulation mass box;
- A power Amplifier DA 200 connected to a vibration exciter;
- An NTI MR2 Analog Audio Signal Generator with functions for external data file uploading from PC generators.

The two dynamic load stages were applied to the simulation mass. Both load stages were in the frequency range of 1 to 20 Hz. The first signal was generated as a continuous sweep, and the second was a stepped sweep with an increase of 1 Hz a step with a duration of 20 sec per step. The excitation was performed with a constant amplitude of vibration displacement.

After the measuring procedure, recorded data was verified through integration processes in the SigView analyzer to see if the vibration displacement amplitude was really constant. In the small amplitude loading process, vehicle vibration can be comparable. After the initial data check, the Operational Modal Analysis Pro evaluation process started as a module of the BK Pulse. This module is based on the ARTEMIS system. Original non-modified, non-filtered recorded data were prepared and transformed into the ARTEMIS data format. After programming, a script with parameters for a run of the dynamic analysis with variable computation settlements was evaluated. Analysis of evaluation enabling by processing system was

- Frequency domain decomposition;
- Enhanced frequency domain decomposition;
- Analysis using curve-fit frequency domain decomposition;
- Stochastic subspace identification—unweighted principal component;
- Stochastic subspace identification—principal component;
- Stochastic subspace identification—canonical variate analysis [34].

5. Results and Discussions

5.1. Quasistatic Test Results

The measuring string was recalibrated before and after each measurement, and the transformation equation between voltage increase and force load was $\Delta F = \Delta I \cdot 118 + 4.28$ [N]. Where ΔI is the voltage increase, and ΔF is the load force increase. The results of the static analysis are represented in Figure 10. This figure shows the relaxation effect of the material for five load stages.

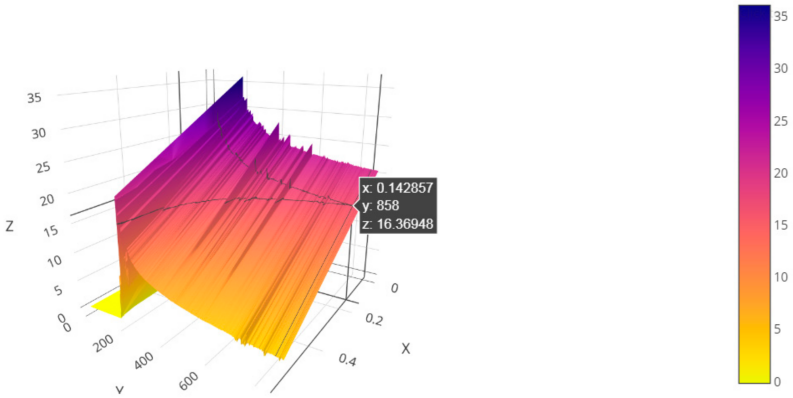

Figure 10. The stress relaxation analysis of material during the static load test, where X-axis is strain stage, Y-axis is time (s) a Z-axis is force (N).

The results of the static load tests are represented in Table 3. This table contains statistically evaluated values of material constants for five load stages. The stages are divided due to the deflection of the rigid disc.

Table 3. Modulus of elasticity as a result of a static plate load test.

Deflection [mm]	ε [-]	F_{inf} [N]	F_{peak} [N]	σ_{inf} [Pa]	σ_{peak} [Pa]	E_{inf} [Pa]	E_{peak} [Pa]
16	0.0400	20.5	36.1	7260	12,761	181,496	319,017
15	0.0357	16.3	32.2	5752	11,399	161,069	319,173
14	0.0327	12.0	28.4	4245	10,041	129,778	306,965
13	0.0298	7.7	24.5	2738	8679	91,818	291,089
12	0.0271	3.5	20.7	1230	7325	45,316	269,792

5.2. Dynamic Test Results

As an example of the identification of dominant frequency bands in the harmonic wave propagation process over the testing surface in Figure 11, the peak detection of overall spectral characteristics can be seen. This figure also shows how the averaged spectrum changed over measuring time—spectrogram.

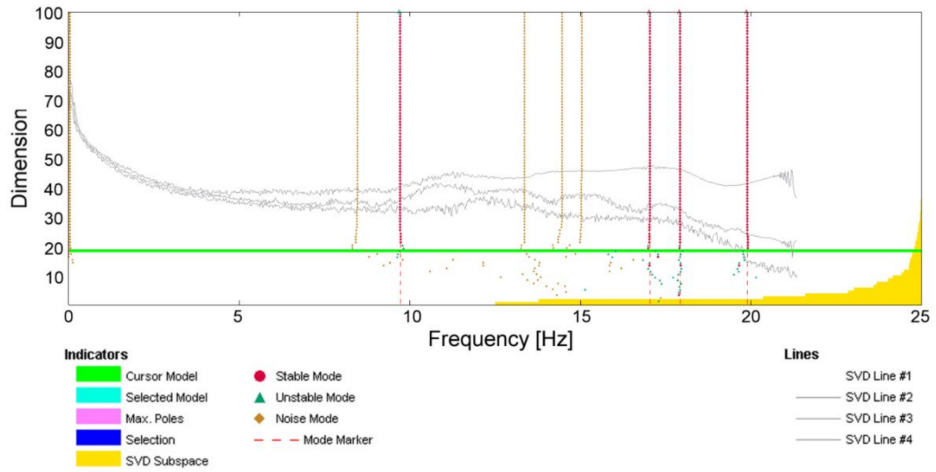

(a)

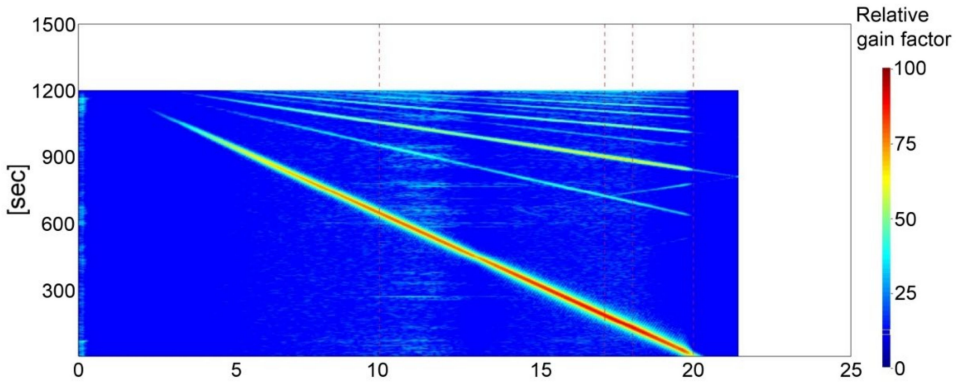

(b)

Figure 11. The frequency transmission identification: (**a**) Peak detection of averaged spectra; (**b**) Spectrogram of the averaged spectrum, where SVD is Singular value decomposition.

The identified frequency peaks, appearing in each method of measurement processing, and the vibration mode shapes are interpreted in Figure 12. Because the reference accelerometer was a rigid disc and there was no damping effect of the simulation mass, the displacement in figures contained strong peaks in the middle of the circular quarter. In the other measured points, however, the wave behavior characteristics could be observed mainly when the mode was animated [35].

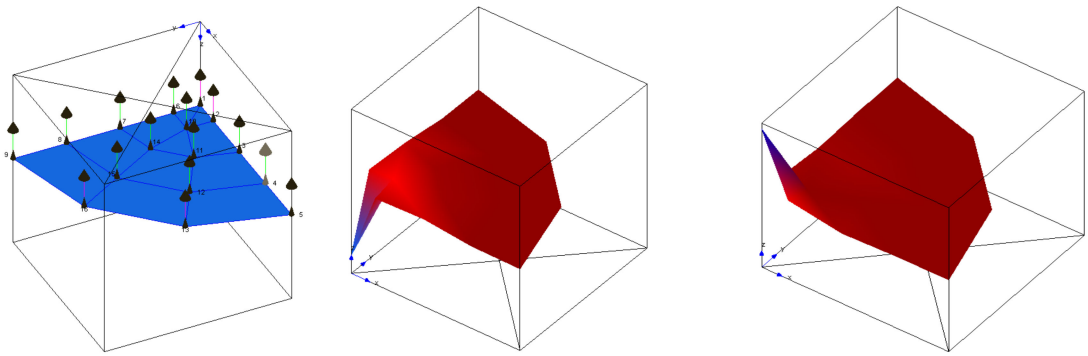

(a) **(b)** **(c)**

Figure 12. The surface experimental model (**a**), the mode shapes for the dominant frequencies $f_{(D1)}$ = 9.5 Hz (**b**) and $f_{(D2)}$ = 17.5 Hz (**c**).

5.3. Discussions

The results of the static load tests are represented in Table 3. Based on these results, we can conclude the following investigation. Total deformation was in good agreement with propagation, which was induced by the simulation mass. The deformation amplitudes corresponded with the FEM (Finite Element Method) model outputs, based on the simple linear elastic material model. The loading stages coincided together in terms of the variable strain. The loading and unloading phases of the stage were almost identical. Peak values of vertical loading forces were in the interval from 2 to 3.6 kg, considering the gravitation acceleration of 9.81 m/s^2. There was an assumption of a small increment of deformation because of the mechanism of the loading apparatus. The viscoelastic nature causes dissipation of the value of peak loading forces. This dissipation is more obvious within an increasing loading interval duration. This phenomenon was proved by the test where F_{inf} was from an interval of 0.3 to 2 kg. Stresses were calculated for the given contact area of the loading plate, and they were related to the forces obtained from the tensometer. Because of sufficient rigidity of the testing equipment, no relaxation was allowed. The modulus of elasticity E characterized the deformation response of the simulation mass to the induced load. The testing aimed to determine two types of elastic moduli: one related to the peak load and the second one related to the infinite values of loading. The moduli's peak values were in the interval from 269 to 319 kPa, which is in good agreement with the previous research. The selection of the appropriate modulus depends on the loading mode applied to the soil body. Short-term cases require high moduli values because of the short-time influences on the soil body [36,37].

In the dynamic investigation of the simulation mass in-labo, all wave processes determined for the real soils or viscoelastic half space could be applied. The behavior of the simulation mass indicated this fact based on dynamic measurements. There were two important frequencies $f_{(D1)}$ = 9.5 Hz and $f_{(D2)}$ = 17.5 Hz. These frequencies impact the potential amplifying properties of the simulation mass model (including fixed steel box border). The analysis was performed for the frequency band close to the dominant frequencies of further simulations (passing the vehicle at physical models). In dominant mode shapes of vibration, a huge damping effect for cross-correlation responses could be observed for distanced points. In the peak detection process using variable evaluating methods, other questionable frequencies also appeared. In these cases, the dumping ratio was unstable or

with large dispersion, and the frequency transmission was not guaranteed. As seen in Figure 11, the spectrogram decelerated the relevant smooth sweep over the whole forced vibration during excitation. The other peak amplitudes in this graphic interpretation (less significant rays) represented reflections and harmonic mirroring [38,39].

6. Conclusions

Based on the performed experimental measurements on the physical model as well as the numerical simulation performed in FEM, we can state that the gelatin-based simulation mass is usable for the simulation of the earth environment in contact with building structures.

The utilization of gelatin-like materials for simulation purposes has not been widely investigated. These materials are defined by specific properties, which are usable for simulating quasistatic and dynamic phenomena. Parameters are highly condition-dependent, but parameters of these materials can be used to describe the real materials when these conditions are specified. As presented in this study, the simulation mass based on gelatin-like material had certain properties, which allowed it to simulate soft materials, such as fine-grained soils. Such soils are often present in the pavement subgrade. This paper contributes to a better understanding of a research area that is not much investigated yet.

The presented study investigated the possibility of applying simulation mass for physical modeling of a pavement. The utilization of this material depends on the determined deformation characteristics that need to be taken into account when selecting the physical scale model. Additionally, the loading mode of the proposed model and appropriate values of moduli should reflect the real case loading mechanism (long-term and short-term conditions). Considering the presented case study described in Chapter 2, it allows a detailed investigation into the mode of transfer mechanism of vibrations through the soil body. The physical and numerical outputs modeling can be extrapolated for real cases, which are usually restrained in terms of survey, design, time, and costs. The results of the research should be added to the standards dedicated to the technical seismicity events.

The variety of conditions encountered in practice, for example, possible slopes of pavement, various materials, potential damage and discontinuities, and the presence of filtration processes, requires a more careful conclusion from the case considered in this research.

Future research in this area involves investigating particular pavement construction layers and the whole pavement structure in mutual interaction. Additionally, the transfer of traffic-induced vibrations and their negative effects on the building structures will be examined.

Author Contributions: Conceptualization, V.V. and J.V.; methodology, V.V., J.V.; software, V.V.; validation, V.V., J.V. and D.P.; formal analysis, V.V., J.V.; investigation, V.V., J.V.; resources, V.V., J.V.; data curation, D.P.; writing—Original draft preparation, writing—Review and editing, visualization, supervision, project administration, funding acquisition, V.V. All authors have read and agreed to the published version of the manuscript.

Funding: This research received no external funding.

Acknowledgments: The project was performed with the financial supported by the conceptual development of science, research, and innovation of the Slovak Grant National Agency VEGA 1/0006/20 by Ministry of Education, Youth, and Sports of the Slovak Republic and financial support of the UNIZA Grant System.

Conflicts of Interest: The authors declare no conflict of interest.

References

1. Fut Park, D.-W.; Papagiannakis, A.T.; Kim, I.T. Analysis of dynamic vehicle loads using vehicle pavement interaction model. *J. Civ. Eng.* **2014**, *18*, 2085–2092. [CrossRef]
2. Czerner, M.; Fellay, L.S.; Suárez, M.P.; Frontini, P.M.; Fasce, L.A. Determination of elastic modulus of gelatin gels by indentation experiments. *Procedia Mater. Sci.* **2015**, *8*, 287–296. [CrossRef]
3. Valaskova, V.; Vlcek, J. Experimental investigation of the vehicle-ground interaction—Experiment preparation and preliminary results. *Civ. Environ. Eng.* **2017**, *13*, 99–105. [CrossRef]
4. Vlcek, J.; Valaskova, V. Analysis of applicability of Clegg impact soil tester for clayey soils. In *XXVII R-S-P Seminar, Theoretical Foundation of Civil Engineering*; EDP Sciences: Les Ulis, France, 2018; pp. 1–7.

5. Scheidl, M.; Chiari, M.; Kaitna, M.; Krawtschuk, A.; Zimmermann, T.; Proske, D. Analysing debris-flow impact models, based on a small scale modelling approach. *Surv. Geophys.* **2013**, *34*, 121–140. [CrossRef]
6. Laurent, J.L.; Janmey, P.A.; Ferry, J.D. Dynamic Viscoelastic Properties of Gelatin Gels in Glycerol—Water Mixtures. *J. Rheol.* **1980**, *24*, 87–97. [CrossRef]
7. Ruiz, A.; Guevara, J. Environmental and Economic Impacts of Road Infrastructure Development: Dynamic Considerations and Policies. *J. Manag. Eng.* **2020**, *36*, 04020006. [CrossRef]
8. Wang, C.; Lim, M.K.; Zhang, X.; Zhao, L.; Lee, P.T.-W. Railway and road infrastructure in the Belt and Road Initiative countries: Estimating the impact of transport infrastructure on economic growth. *Transp. Res. Part A Policy Pract.* **2020**, *134*, 288–307. [CrossRef]
9. Noland, R.B. Traffic fatalities and injuries: The effect of changes in infrastructure and other trends. *Accid. Anal. Prev.* **2003**, *35*, 599–611. [CrossRef]
10. Pamanikabud, P.; Tansatcha, M. 3D analysis and investigation of traffic noise impact from a new motorway on building and surrounding area. *Appl. Acoust.* **2010**, *71*, 1185–1193. [CrossRef]
11. Tong, Z.; Chen, Y.; Malkawi, A.; Adamkiewicz, G.; Spengler, J.D. Quantifying the impact of traffic-related air pollution on the indoor air quality of a naturally ventilated building. *Environ. Int.* **2016**, *89–90*, 138–146. [CrossRef]
12. Van Bohemen, H.D.; Van de Laak, W.H.J. The influence of road infrastructure and traffic on soil, water, and air quality. *Environ. Manag.* **2003**, *31*, 50–68. [CrossRef] [PubMed]
13. François, S.; Pyl, L.; Masoumi, H.R.; Degrande, G. The influence of dynamic soil–structure interaction on traffic induced vibrations in buildings. *Soil Dyn. Earthq. Eng.* **2007**, *27*, 655–674. [CrossRef]
14. Korkmaz, K.A.; Ay, Z.; Keskin, S.N.; Ceditoglu, D. Investigation of traffic-induced vibrations on masonry buildings in turkey and countermeasures. *J. Vib. Control.* **2010**, *17*, 3–10. [CrossRef]
15. Persson, P.; Andersen, L.V.; Persson, K.; Bucinskas, P. Effect of structural design on traffic-induced building vibrations. In Proceedings of the X International Conference on Structural Dynamics, EURODYN 2017, Rome, Italy, 10–13 September 2017; Elsevier: Amsterdam, The Netherlands, 2017.
16. European Union. *EN 1998-1: Eurocode 8: Design of Structures for Earthquake Resistance—Part 1: General Rules, Seismic Actions and Rules for Buildings*; European Committee for Standardization: Brussels, Belgium, 2004.
17. Bencat, J.; Stypula, K. Buildings structure response due to railway traffic. *Commun.-Sci. Lett. Univ. Zilina* **2013**, *15*, 41–48.
18. Al-Defae, A.H.; Knappett, J.A.; Brown, M.J. Small-scale modelling of reinforced concrete for physical model tests, and its application in centrifuge testing of a soil-structure interaction problem. In Proceedings of the 1st International Conference on Natural Hazards & Infrastructure, Chania, Greece, 28–30 June 2016.
19. Dhaybi, M.; Pellet, F. Physical modelling of a small scale shallow foundation reinforced by Soil-Mixing. In Proceedings of the Second International Conference on Geotechnique, Construction Materials and Environment, Kuala Lumpur, Malaysia, 14–16 November 2012; Springer: New York, NY, USA, 2012.
20. Heib, M.A.; Emeriault, F.; Caudron, M.; Nghiem, L. Large-scale soil-structure physical model (1g)—Assessment of structure damages. *Int. J. Phys. Model. Geotech.* **2013**, *13*, 138–152. [CrossRef]
21. Heib, M.A.; Emeriault, F.; Nghiem, H.L. On the use of 1g physical models for ground movements and soil-structure interaction problems. *J. Rock Mech. Geotech. Eng.* **2020**, *12*, 197–211. [CrossRef]
22. Sulaeman, A.; Ling, F.N.L.; Sajiharjo, M. Modelling of clay behaviour in pile loading test using one-gravity small-scale physical model. *Appl. Mech. Mater.* **2015**, *773–774*, 1535–1541. [CrossRef]
23. Tasevska, M.; Susinov, B.; Josifovski, J. Small-scale physical and numerical modelling of slope failure in sand. In Proceedings of the 7th International Conference on Business, Technology and Innovation, Pristina, Kosovo, 26–28 October 2018. [CrossRef]
24. Vereecken, H.; Schnepf, A.; Hopmans, J.; Javaux, M.; Or, D.; Roose, T.; VanderBorght, J.; Young, M.; Amelung, W.; Aitkenhead, M.; et al. Modeling soil processes: Review, key challenges, and new perspectives. *Vadose Zone J.* **2016**, *15*, 1–57. [CrossRef]
25. Martino, R. Modelling and Simulation of the Dynamic Behaviour of the Automobile. Ph.D. Thesis, Université de Haute Alsace, Mulhouse, France, 20 September 2005.
26. Beiser, A. *Perspectives of Modern Physics*; Academia: Praha, Czech Republic, 1978.
27. Gunzler, H.; Gremlich, H.U. *IR Spectroscopy, An introduction*; Willey-VCH Verlag GmbH: Weinheim, Germany, 2002; 361p, ISBN 3-527-28896-1.

28. Wolkers, W.F.; Oliver, A.E.; Tablin, F.; Crowe, J.H. A Fourier-transform infrared spectroscopy study of sugar glasses. *Carbohydr. Res.* **2004**, *339*, 1077–1085. [CrossRef]
29. Araghipour, N.; Colineau, J.; Koot, A.; Akkermans, W.; Rojas, J.M.M.; Beauchamp, J.; Wisthaler, A.; Märk, T.D.; Downey, G.; Guillou, C.; et al. Geographical origin classification of olive oils by PTR-MS. *Food Chem.* **2008**, *108*, 374–383. [CrossRef]
30. Zhou, W.; Liu, H.; Xu, Q.; Li, P.; Zhao, L.; Gao, H. Glycero's generalized two-dimensional correlation IR/NIR spectroscopy and its principal component analysis. *Spectrochim. Acta Part A Mol. Biomol. Spectrosc.* **2020**, *228*. [CrossRef] [PubMed]
31. Shimokawa, Y.; Hayakawa, E.; Takahashi, K.; Okai, K.; Hattori, Y.; Otsuka, M. Pharmaceutical formulation analysis of a gelatin-based soft capsule film sheet containing phytic acid using near-infrared spectroscopy. *J. Drug Deliv. Sci. Technol.* **2019**, *53*, 101126. [CrossRef]
32. Deutsches Institut für Normung. *Soil—Testing Procedures and Testing Equipment, Plate Load Test*; German Institute for Standardisation: Berlin, Germany, 2012.
33. Germoso, C.; Duval, J.L.; Chinesta, F. Harmonic-Modal Hybrid Reduced Order Model for the Efficient Integration of Non-Linear Soil Dynamics. *Appl. Sci.* **2020**, *10*, 6778. [CrossRef]
34. Ruzzo, C.; Failla, G.; Collu, M.; Nava, V.; Fiamma, V.; Arena, F. Operational modal analysis of a spar-type floating platform using frequency domain decomposition method. *Energies* **2016**, *9*, 870. [CrossRef]
35. Linehan, D.; Napolitano, K. A Comparison of Accelerometer Selection Methods for Modal Pretest Analysis. In *Modal Analysis Topics, Proceedings of the 29th IMAC, A Conference on Structural Dynamics, Jacksonville, FL, USA, 31 January–3 February 2011*; Conference Proceedings of the Society for Experimental Mechanics Series; Proulx, T., Ed.; Springer: New York, NY, USA, 2011; Volume 3. [CrossRef]
36. Parida, A.; Sarangi, S.; Jayashree, B. Study the modulus elasticity of HFRC. *J. Ind. Pollut. Control* **2017**, *3*, 1209–1213.
37. Davarpanah, S.M.; Van, P.; Vásárhelyi, B. Investigation of the relationship between dynamic and static deformation moduli of rocks. *Géoméch. Geophys. Geo-Energy Geo-Resour.* **2020**, *6*, 1–14. [CrossRef]
38. Papánová, Z. Soil-Structure dynamic interaction experimental analysis due to railway traffic. In Proceedings of the International Multidisciplinary Scientific GeoConference-SGEM, Albena, Bulgaria, 17–26 June 2014; Volume 1, pp. 605–612.
39. Luo, M.; Wang, H.; Chen, X.; Zhai, Y. Structure-soil-structure interaction: Literature review. *Soil Dyn. Earthq. Eng.* **2011**, *31*, 1724–1731. [CrossRef]